Title

Super-resolution surface slope metrology of x-ray mirrors

Journal

Review of Scientific Instruments, 91(7)

ISSN

0034-6748

Authors

Yashchuk, Valeriy V

Rochester, Simon

Lacey, Ian

et al.

Publication Date

2020-07-01

DOI

10.1063/5.0005556

Peer reviewed

Review of Scientific Instruments

Super-resolution surface slope metrology of x-ray mirrors

Valeriy V. Yashchuk,[1,a)] Simon Rochester,[2] Ian Lacey,[1] and Sergey Babin[3]

[1]*Advanced Light Source, Lawrence Berkeley National Laboratory, Berkeley, CA, 94720, U.S.A.*
[2]*Rochester Scientific LLC., El Cerrito, CA 94530, U.S.A.*
[3]*aBeam Technologies, Inc., Hayward, California 94541, USA*

We present experimental, analytical, and numerical methods developed for reconstruction (deconvolution) of one-dimensional (1D) surface slope profiles over the spatial frequency range where the raw data are significantly perturbed due to the limited resolution of the measurement instrument. We characterize the spatial resolution properties of a profiler with the instrument's transfer function (ITF). To precisely measure the ITF, we apply a recently developed method utilizing test surfaces with 1D linear chirped height profiles of constant slope amplitude. Based on the results of the ITF calibration, we determine parameters of an analytical model for the ITF that is used in original reconstruction software. Here, we treat surface slope metrology data obtained with the Optical Surface Measuring System (OSMS), using as a sensor an electronic autocollimator (AC) ELCOMAT-3000. The spatial resolution of the OSMS is limited by the size of the AC light-beam-collimating aperture. For the purposes of this investigation, the OSMS is equipped with a circular aperture with a diameter of 2.5 mm. This is a typical arrangement of most AC-based slope profilers developed for surface slope metrology of state-of-the-art x-ray mirrors. Using the example of surface slope metrology of two state-of-the-art elliptically shaped x-ray focusing mirrors, we demonstrate that the developed data reconstruction procedure allows us to significantly improve the accuracy of surface slope metrology with the OSMS over the spatial wavelength range from ~1.6 mm to 7 mm. Thus, the amplitude of the quasi-periodic error characteristic of the deterministic polishing process used appears to be higher by a factor of ~2 than is apparent from the rough metrology data. Underestimation of the surface slope errors in this spatial wavelength range can lead to serious errors in the expected performance of x-ray mirrors in synchrotron beamlines, especially at modern light sources utilizing coherent x-rays, where the perturbations can lead to increased speckle-like intensity variation.

[a)] Electronic mail: vvyashchuk@lbl.gov.

I. INTRODUCTION

We present experimental, analytical, and numerical methods, constituting a multistep procedure, developed for reconstruction (deconvolution) of one-dimensional (1D) surface slope distribution functions (profiles) of the surface topography (also referred as '1D surface slope topography), inherent to the surface of an x-ray mirror under test. The developed procedure allows us to reconstruct (at least partially) the 1D surface slope data over the spatial frequency range, where the raw (measured) data are significantly perturbed due to the limited resolution of the instrument in use. A possibility for the reconstruction of oversampled 1D surface slope data has recently been discussed[1] in application to the artificial data generated as a result of a stochastic polishing process.[2-5]

The reconstruction procedure, described in the present paper, is based on the known (precisely measured, analytically modeled, and parametrized) instrument's point spread function (PSF) and/or instrument's transfer function (ITF), related to each other through the Fourier transform.

For the characterization of the resolution of surface slope profilers, different periodic and chirped profiles have been discussed in the literature.[6-10] In order to obtain direct information on a profiler's ITF, we use specially designed chirped slope test samples.[8-10] The 1D surface height variation of the sample has constant (independent of spatial frequency) slope (rather than height) amplitude.[9] When a direct measurement of the PSF and ITF is not possible, the recently developed methods (see Refs.[11-21] and references therein) for precision calibration of the modulation transfer function (MTF) of different metrology tools can provide data needed for the reconstruction.

In this paper, we treat 1D surface slope metrology data of several high-quality x-ray mirrors measured with the Optical Surface Measuring System (OSMS),[10,22,23] recently brought into operation at the Advanced Light Source (ALS) X-Ray Optics Laboratory (XROL).[24,25]

The OSMS is a surface slope profiler based on an electronic autocollimator (AC) ELCOMAT-3000.[26] The same ACs are used as optical slope sensors in the Nanometer Optical Measuring Machine (NOM), originally developed at the HZB/BESSY-II.[27,28] Most of the optical metrology labs at synchrotron and free-electron-laser x-ray facilities have AC-based profilers in different arrangements.[29-35] These tools have proven capable of characterizing ultraprecise aspherical x-ray optics with an accuracy on the level of 50-100 nrad root-mean-square (rms).

The spatial resolution of the AC-based slope profilers is limited by the size of the AC light-beam collimating aperture. Similar to the XROL OSMS arrangement in this paper, a circular aperture with a diameter of about 2.5 mm is typically used. A smaller aperture diameter leads to an increase of the profiler's systematic error and loss of stability (repeatability) of the measurements.[36,37] Performance of the AC-based profilers with apertures of different shapes and sizes have been investigated in Ref.[10]

The ITF characterization of the OSMS is performed with the chirped slope test sample.[8-10] The sample has two chirped slope profiles with lower and higher spatial frequencies (here, we use the latter one). The inherent height profiles of the sample were accurately measured with a large aperture Fizeau interferometer[10] and numerically differentiated to get the corresponding slope variations. Fabrication of such a sample with a variation of the height amplitude down to a few nanometers is a challenging task.[38] As a result, the inherent slope variation amplitude of the chirped profiles is nearly, but not exactly, constant. Nevertheless, the fabricated sample[8,9] allows very sophisticated characterization of slope profiles with different experimental arrangements.[10,39]

Due to the limited spatial resolution of the OSMS, the ratio of the measured slope variation amplitude to that of the inherent surface profile dramatically decreases with an increase of the slope variation frequency.[9,10] Thus, where the spatial period of slope variation is about 6 mm, the

profiler's error in the variation amplitude is only about 10%, while at a 2-mm period, it reaches a factor of almost 3. This range of spatial wavelengths is of special importance for state-of-the-art aspherical x-ray optics fabricated with deterministic polishing techniques. It appears that such optics often have quasi-periodic surface errors with characteristic spatial wavelengths between about 2 and 8 mm.[40,41] Underestimation of the surface slope errors in this spatial wavelength range can lead to serious errors in the expected performance of the optics in beamlines, especially when utilizing coherent x-rays.

The data reconstruction procedure described in the present paper allows partial remediation of the resolution limitation of surface slope profilers.

This paper is organized as follows: The mathematical foundations for partial reconstruction of the measured data, accounting for measurement error due to the profiler's ITF, are briefly outlined in Sec. II. The reconstruction is based on application of approximate correction methods developed for restoration of blurred images as suggested by Norbert Wiener.[42,43] The key features of the original software SlopeReconstruction1D^{TM} developed in the Python 3 environment are also briefly overviewed in Sec. II. In Sec. III, we apply the software to parametrize the OSMS ITF based on calibration measurements made with the chirped slope test sample. In processing the ITF calibration data, we also determine the optimal parameters for the reconstruction routine. The results of reconstruction of tangential slope data measured with two state-of-the-art elliptically-shaped x-ray mirrors are discussed in Sec. IV. We show that in spite of the fact that after the reconstruction, the residual slope error (after subtraction of the best-fit elliptical shape) is just slightly larger, though the power spectral density (PSD) peaks of the quasi-periodic surface slope variation, characteristic for the deterministic polishing process used for the mirror fabrication,

appear to be higher by a factor of up to ~4.5. We conclude (Sec. V) by summarizing the main concepts discussed through the paper and outlining a plan for future work.

II. MATHEMATICAL FOUNDATIONS OF 1D DATA RECONSTRUCTION

A. PSF and ITF of AC-based slope profiler equipped with circular aperture

Due to the axially symmetric shape of the probe light beam and the point-by-point data acquisition, AC-based slope profilers are linear and shift invariant surface metrology instruments. As such, the spatial resolution properties of the OSMS can be characterized by the instrument's point spread function $PSF(x)$ that describes its response to a point (delta-function-like) slope topographic object.[44-46] Consistently, a 1D surface slope profile measured with the OSMS, can be expressed as a convolution of the $PSF(x)$ with the slope trace $\alpha_{SUT}(x)$, corresponding to the inherent (unperturbed by the measurement) topography of the surface under test (SUT):

$$\alpha_{MES} = PSF * \alpha_{SUT} + \varepsilon_{MES}\,, \tag{1}$$

where $\alpha_{MES} \equiv \alpha_{MES}(x)$ is the measured trace and the symbol '*' denotes the convolution operation. The additive noise ε_{MES} is due to random errors of the measurement, such as, for example, the detector dark-current noise. For simplicity of the discussion in this section, we assume that measurement drift and systematic errors are negligible.

The ITF is defined as the Fourier transform ($\mathsf{F}[\ldots]$) of the PSF,[44]

$$ITF = \mathsf{F}[PSF]\,. \tag{2}$$

Simplified analytical expressions for modeling the 1D PSF and ITF of an AC-based slope profiler equipped with a circular aperture, assuming a uniform distribution of the sensing light over the aperture, are presented in Refs.:[1,10]

$$PSF(x) \equiv PSF_x = \frac{2\sqrt{a^2 - x^2}}{\pi a^2} H\left[a^2 - x^2\right], \tag{3}$$

$$ITF(u) \equiv ITF_u = \frac{J_1(2\pi a u)}{\pi a u}, \tag{4}$$

where $H[z]$ is the Heaviside step function (equal to zero for negative z and one for positive z),[47] J_1 is the first order Bessel function of the first kind, u is the spatial frequency variable, corresponding to the coordinate x, and a is the radius of the aperture.

The ITF given by Eq. (4) produces a low-pass filtering effect, and so the resolution of the measuring instrument is usually defined according to the first zero of the ITF. However, although the slope information about the SUT is completely lost at the frequencies of the multiple zeros of the ITF, the nonzero regions above the first zero (including both the positive regions and the negative regions of the ITF where the contrast is reversed) do preserve information. This suggests that a significant portion of the high spatial-frequency information above the nominal instrument resolution can still be reconstructed, if the slope trace is measured with oversampling (that is, with an increment significantly smaller than the instrumental resolution) (see, for example, Refs.[42,43,48,49] and Sec. II B, below).

Note that the PSF given with Eq. (3) is different from the rectangular gate function that one would expect in the case of pure 1D instrument with a finite resolution due to the 1D gate-like aperture. For such a pure 1D instrument, the ITF is described by a sinc function. Similarly, for a 2D rectangular aperture the ITF is a product of two sinc functions.[45,46]

Equations (3) and (4) are obtained under assumption of a uniform distribution over the circular aperture of the AC light sensing the SUT. This assumption is not directly applicable to

ELCOMAT-3000 autocollimators. A more reliable analytical expression for the OSMS ITF, empirically deduced based on the ITF measurements, is presented in Sec. III.

B. Methods for approximate reconstruction of measured data

Applying a Fourier transform to the convolution relation (1), one finds

$$\begin{aligned} \mathsf{F}[\alpha_{MES}] &= \mathsf{F}[PSF]\cdot\mathsf{F}[\alpha_{SUT}] + \mathsf{F}[\varepsilon_{MES}] \\ &= ITF(u)\cdot\mathsf{F}[\alpha_{SUT}] + \mathsf{F}[\varepsilon_{MES}]. \end{aligned} \tag{5}$$

Formally, if the instrument's transfer function $ITF(u)$ is known and reversible, one can derive an estimate $\mathsf{F}[\tilde{\alpha}_{SUT}]$ for the Fourier transform of the inherent surface slope trace α_{SUT} from a straightforward algebraic transformation of Eq. (5):

$$\mathsf{F}[\tilde{\alpha}_{SUT}] \approx \frac{\mathsf{F}[\alpha_{MES}]}{ITF} = \mathsf{F}[\alpha_{SUT}] + \frac{\mathsf{F}[\varepsilon_{MES}]}{ITF}. \tag{6}$$

The next formal step to recover α_{SUT} is to apply the inverse Fourier transform (F^{-1}) to Eq. (6):

$$\tilde{\alpha}_{SUT} \approx \mathsf{F}^{-1}\left[\frac{\mathsf{F}[\alpha_{MES}]}{ITF}\right] = \alpha_{SUT} + \mathsf{F}^{-1}\left[\frac{\mathsf{F}[\varepsilon_{MES}]}{ITF}\right]. \tag{7}$$

Such an approach and its multiple variations have been developed for reduction of image blurring (see, for example, Refs.[42,43,48,49]).

When the error term is equal to zero, $|\mathsf{F}[\varepsilon_{MES}]| \equiv \sigma_{\varepsilon} = 0$, Eq. (7) provides an exact solution.

However, at non-zero error, the result of recovery tends to be particularly sensitive to measurement error. At the spatial frequencies where the ITF is significantly small, the function ITF^{-1} can lead to strong enhancement of the error term and, therefore, to corruption of the reconstruction. Moreover, in general the ITF has, besides multiple zeros, negative regions that result in severe perturbation of the measured trace due to the reverse of the contrast at these spatial frequencies. This is the case of the OSMS ITF (see Sec. III).

The sensitivity to the error term in Eqs. (6) and (7) can be reduced by limiting ITF^{-1} to some threshold ξ and ignoring the regions where the error term dominates:

$$S(u) = \begin{cases} ITF^{-1}, & \text{if} \quad ITF > \xi \\ \xi \cdot |ITF| \cdot ITF^{-1}, & \text{otherwise.} \end{cases} \tag{8}$$

The threshold inverse ITF $S(u)$ given by Eq. (8) can be optimized by careful selection of ξ. For a higher degree of optimization, the Wiener optimal filter can be employed.[42,43]

When applied to the reconstruction of 1D surface slope topography of x-ray mirrors, the Wiener optimal filter minimizes the mean square error between the reconstruction $\tilde{\alpha}_{SUT}$ and the inherent surface distribution α_{SUT}. Due to the unitary property of the Fourier transform, there is the same information in the real and Fourier domains. Therefore, if $\tilde{\alpha}_{SUT} \approx \alpha_{SUT}$, the corresponding Fourier transforms are also close, $\mathsf{F}[\tilde{\alpha}_{SUT}] \approx \mathsf{F}[\alpha_{SUT}]$, and the least squares method can be applied in the Fourier domain. The minimization variable is the inverse ITF $S(u)$ [compare with Eq. (6)]:

$$\mathsf{F}[\tilde{\alpha}_{SUT}] = \mathsf{F}[\alpha_{MES}]S(u) = \mathsf{F}[\alpha_{SUT}]\, ITF(u)\, S(u) + \mathsf{F}[\varepsilon_{MES}]S(u), \tag{9}$$

so that

$$\frac{\partial}{\partial S}\left\langle \left| \mathsf{F}[\alpha_{SUT}] - \mathsf{F}[\tilde{\alpha}_{SUT}] \right|^2 \right\rangle = 0. \tag{10}$$

Substitution of (9) into (10) gives

$$\frac{\partial}{\partial S}\left\langle \left| \mathsf{F}[\alpha_{SUT}] - \mathsf{F}[\alpha_{SUT}]\, ITF(u)\, S(u) - \mathsf{F}[\varepsilon_{MES}]S(u) \right|^2 \right\rangle = 0. \tag{11}$$

Using straightforward algebraic transformation and assuming an independent and zero-mean error distribution, one can derive the Wiener optimal filter expressed through the corresponding PSDs in the following form:[42]

$$S(u) = \frac{ITF^*}{|ITF|^2 + \dfrac{|\mathrm{F}[\varepsilon_{MES}]|^2}{|\mathrm{F}[\alpha_{SUT}]|^2}} = \frac{ITF^*}{MTF^2 + \dfrac{PSD[\varepsilon_{MES}]}{PSD[\alpha_{SUT}]}}, \tag{12}$$

where ITF^* is the complex conjugate of ITF, PSD is the power spectral density, and MTF is the modulation transfer function defined as[44]

$$ITF \equiv MTF \exp(-i\,PTF), \tag{13}$$

where PTF is the phase transfer function (PTF). For a symmetric PSF centered on the ideal image point, the PTF as a function of spatial frequency can have only a value of either zero or π.[44] This is the case of surface slope topography measurements with the OSMS. Correspondingly, the ITF of the OSMS is a real-valued function, which can be bipolar with regions of positive and negative values, and with zero value between them; whereas the MTF is only positively defined. Obviously, in this case $ITF^2 = MTF^2$.

Because of the approximate character of the outlined methods, the reconstructed distribution $\tilde{\alpha}_{SUT}$ is not exactly equal to the inherent α_{SUT}. However, if the reconstruction is successful, the resulting $\tilde{\alpha}_{SUT}$ contains additional and significant information about the inherent surface slope distribution α_{SUT} that is not directly seen in the measured trace α_{MES}.

C. Numerical methods for reconstruction of 1D surface slope data

In this section, we outline the numerical methods placed in the foundation of the dedicated software SlopeReconstruction1D™ developed for reconstruction of 1D surface slope metrology data. We also briefly review the major features of the software.

Practical application of the Wiener optimal filter via Eq. (12) needs to overcome the fact that the PSDs of the inherent trace α_{SUT} and the measurement error ε_{MES} are generally unknown. There

are a number of possible approximations.[43] The one employed here consists in replacement of the term $PSD[\varepsilon_{MES}]/PSD[\alpha_{SUT}]$ in the denominator of Eq. (12) by a regularization parameter multiplied by the PSD of a preselected "regularization operator." Here, we have chosen the discrete Laplace operator,[48] defined by the kernel [-1, 2, -1]. The PSD of this operator is zero at zero frequency and rises to a maximum at the Nyquist frequency. As used in the Wiener filter, this has the effect of de-emphasizing high frequencies in the reconstruction solution, promoting stability.

Figure 1 shows the application window of SlopeReconstruction1D™ software with the example of treatment of the OSMS data measured with the chirped test sample (for more detail discussion, see Sec. III).

In Fig. 1, the reconstructed intrinsic chirped slope profile is shown with the green dotted line, the blue solid line depicts the surface slope distribution of the chirped test sample as measured with the OSMS, and the red dashed line corresponds to the slope distribution obtained by convolution of the intrinsic chirped slope profile (see Sec. III A); this is the processed data. For the convolution, the 'Convolve intrinsic' operation mode of the SlopeReconstruction1D™ software is used.

The principal "Operation" control is the "Deconvolve measured" mode used for reconstruction of the measured data based on the selected analytical model of the PSF or ITF. The "Convolve intrinsic" mode (depicted in Fig. 1) allows convolving a loaded intrinsic data file with the currently selected PSF. This mode helps to determine the parameters of the ITF used in data reconstruction.

Either the PSF or the ITF can be specified for the convolution of the intrinsic, or reconstruction of the measured data; the other of the two is calculated using the Fourier transform.

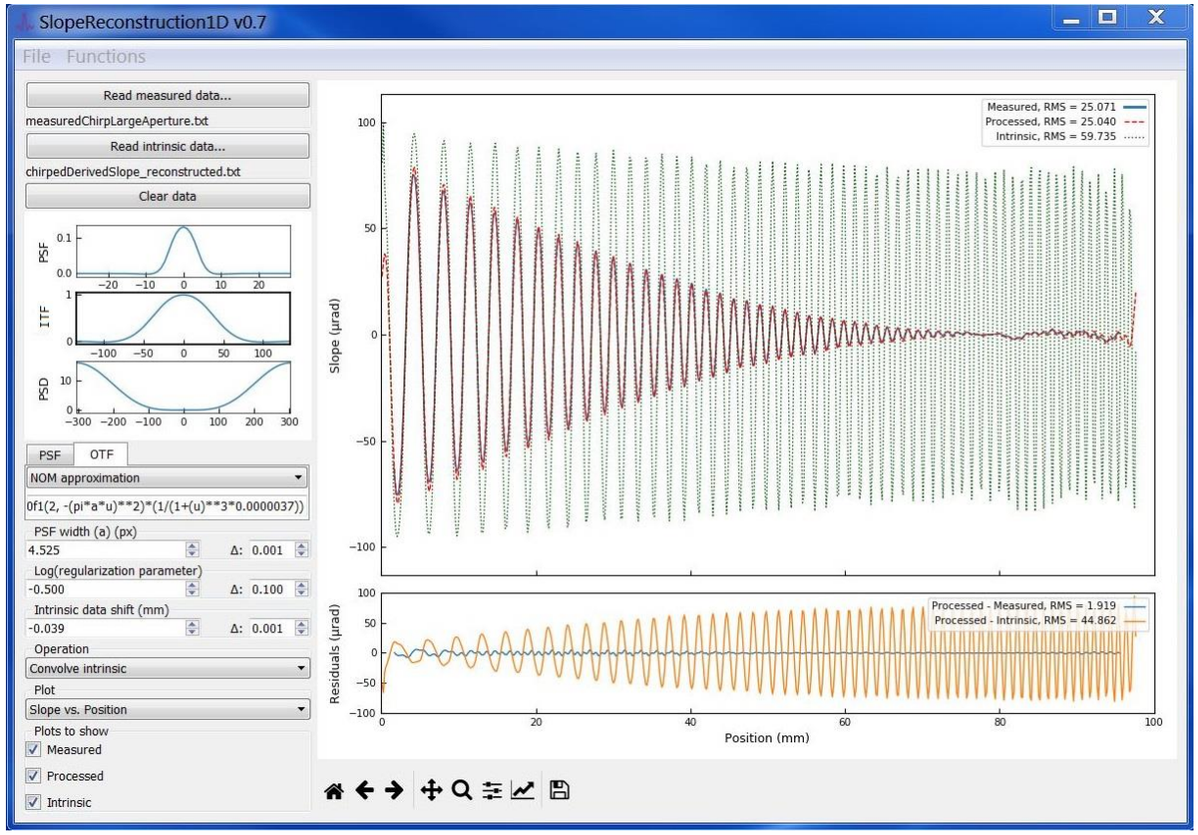

Fig. 1. Application window of the reconstruction software SlopeReconstruction1D™ with the example of treatment of the OSMS data measured with the chirped test sample (for a detailed explanation, see the text).

A list of the built-in PSFs includes Gaussian filter (Gaussian ITF), gate-function (sinc-function ITF), and the circular aperture PSF given with Eq. (3) [the corresponding ITF is given with Eq. (4)]. The list of predefined analytical functions can be expanded with additional user-defined functions. In Fig. 1, an empirical approximation (discussed in Sec. III B) of the OSMS ITF is shown.

The effective usage of the software requires the high-confidence selection of various numeric parameters: the PSF width parameter, the logarithm of the regularization parameter, and an optional lateral shift of the intrinsic data. Section III C describes such a selection.

The software data presentation ("Plot" control) has two options, "Slope vs Position" (depicted in Fig. 1) and "Slope PSD." The latter option provides the capability to treat the measured, inherent, and processed (convolved or recovered) data in the spatial frequency (PSD) domain. This feature helps to verify the selection of the parameters of the reconstruction routine and to better understand the spatial frequency range of the recovered data (see discussion in Sec. III C).

III. PARAMETRIZATION OF THE OSMS ITF

Here, we discuss the use of the developed reconstruction algorithms and software to parametrize the OSMS ITF based on its calibration measurements with the chirped slope test sample.[10] In processing the ITF calibration data, we also determine the parameters used for reconstruction of the OSMS slope metrology data obtained with x-ray mirrors (Sec. IV).

A. The inherent slope variation of the chirped test sample

Precision calibration of the ITF requires highly accurate knowledge of the inherent slope variation of the chirped sample. In our case, the slope profile of the chirped sample is obtained by numerical differentiation of the sample height profile measured with a 6-inch aperture Fizeau interferometer.[10] In these measurements, the effective pixel size of the interferometer is 160.9 μm, much smaller than the expected resolution of the OSMS AC with an aperture of 2.5-mm diameter. However, the numerical differentiation of the high-resolution surface height distribution requires a few height points to obtain each slope point. This leads to an effective filtering of the resulting slope data, decreasing its spatial frequency range. A comprehensive consideration of questions related to numerical differentiation and integration can be found, for example, in Refs.[50,51] Here, in order to decrease the effect of random measurement error, we compute the differential as the symmetric difference quotient of the height trace after cubic-spline smoothing using Mathematica.™

In Fig. 2, the effect of the filtering is seen as a difference between the initially measured height distribution (the red dashed line) and the height distribution, calculated by numerical integration of the slope profile obtained by differentiation of the measured height distribution (the blue solid line).

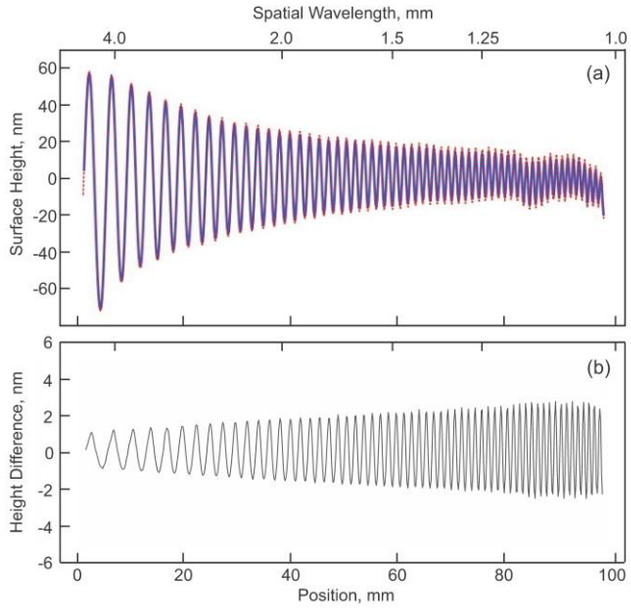

Fig. 2. (a) Surface height distributions of the chirped sample directly measured with the interferometer (the red dashed line) and calculated by re-integration of the slope trace obtained by differentiation of the measured height distribution (the blue solid line); (b) the difference of the height distributions in plot (a).

In order to retrieve the inherent slope profile of the chirped sample, we model the effect of the differentiation with a gate-function PSF (sinc-function ITF) and apply the developed reconstruction procedure and software. The effective width (in number of pixels) of the filter of 2.444 pixels is determined by matching the height distribution, re-integrated from the reconstructed inherent slope profile, to the distribution, directly measured with the interferometer.

Figure 3 depicts the result of the reconstruction in the spatial (slope) and spatial frequency (slope PSD) domains. As expected (see Fig. 2b), the effect of filtering upon numerical differentiation has a strong dependence on spatial frequency, leading to about 40% suppression of

the PSD amplitude at the highest spatial frequencies (around 0.9 mm^{-1}) characteristic to the chirped sample in use. The reconstruction procedure reduces the rms variation of the difference between the processed and directly measured height distributions to 0.033 nm, much smaller than the initial rms variation of 1.5 nm of the difference trace in Fig. 2b. The performed reconstruction allows us to mitigate the effect of the filtering and correct the inherent slope profile of the sample, ensuring the high precision of the ITF calibration of the OSMS.

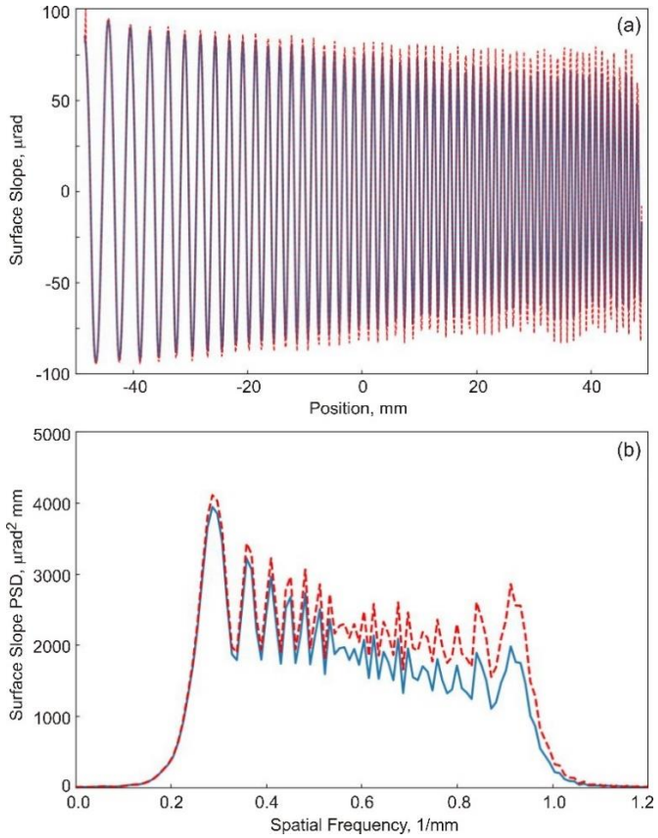

Fig. 3. (a) The slope distributions and (b) the PSD spectra of the chirped slope test sample as the result of differentiation of the height distribution measured with the Fizeau interferometer (the blue solid lines) and reconstructed with the SlopeReconstruction1D^{TM} software (the red dashed line). For the reconstruction, the gate-function PSF (sinc-function ITF) with the filter width of 2.444 pixels was used.

Finally, the inherent chirped slope variation is obtained from the reconstructed trace by correcting it for the quadratic geometric aberration of the interferometer, appearing as a second-

order-polynomial distribution of the pixels (points) of the surface height variation measured with the interferometer. A detailed discussion of the aberration correction can be found in Ref.[39]

B. ITF of the OSMS AC with 2.5-mm circular aperture

In Sec. II, we indicated that the analytical expressions (3) and (4) for the 1D PSF and ITF derived in Ref.[1] based on the simplified model of a slope profiler with a uniformly illuminated circular aperture are not directly applicable to the OSMS with an AC ELCOMAT-3000 equipped with 2.5-mm diameter aperture.

This is illustrated by Fig. 4, which depicts with the red dashed line the result of filtering of the inherent slope profile of the chirped sample with the ITF given by Eq. (4). The filtered (convolved) trace should be compared with the chirped slope profile measured with the OSMS (the blue solid line in Fig. 4). For reference, the inherent chirped slope trace is shown with the green dotted line. The OSMS measurements were performed with the increment of 0.1 mm.

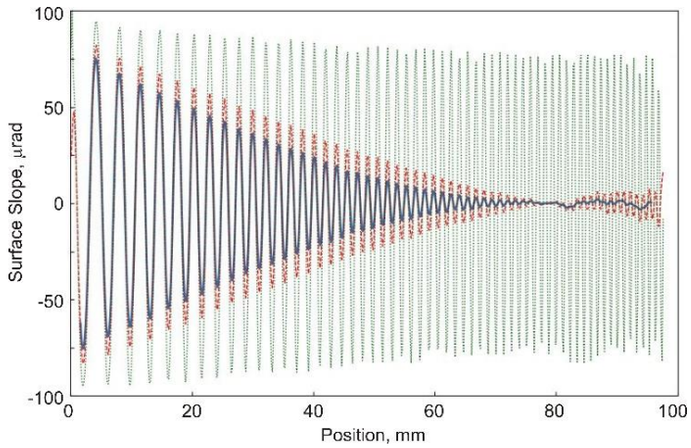

Fig. 4. The slope distributions of the chirped sample as measured with the OSMS AC equipped with 2.5-mm diameter aperture (the blue solid lines) and (the red dashed line) as resulting from the convolution of the corrected inherent slope distribution (shown with the green dotted line) with the circular-aperture ITF, given by Eq. (4) with the effective diameter $2a = 1.456$ mm.

The parameters of the ITF in Fig. 4 were determined as follows. Using the "Convolve intrinsic" operation mode of the reconstruction software, we vary the radius parameter of the circular

aperture ITF and find that the value of $a = 4.525$ pixels provides the best coincidence of the position of the phase flip between the convolved intrinsic and the measured slope traces. Because the increment of the inherent trace is 0.1609 mm, the best-matched effective diameter of the ITF is $2a = 1.456$ mm. This value is in excellent agreement with the previous estimations of the spatial resolution of the slope profilers, based on the ELCOMAT-3000 autocollimator equipped with 2.5-mm diameter aperture.[8-10]

In spite of the fact that the circular-aperture ITF given by Eq. (4) reproduces the overall shape of the OSMS ITF, there is a significant discrepancy seen in Fig. 4 as a systematic excess of the oscillation amplitude of the convolved slope trace. The discrepancy is expected. The simple circular-aperture model does not account for the reticle light intensity distribution and rather complicated procedure for extraction of the value of the measured angle implemented in ELCOMAT-3000 autocollimators.[52] To the best of our knowledge, there is no published analytical description of the ELCOMAT-3000 autocollimator equipped with 2.5-mm diameter aperture that can be used for better modeling its ITF. Therefore, we use the simple model given by Eq. (4) but assume that the parameter a is an effective aperture radius, allowing it to vary. The value of the parameter is determined by matching the deflection points (the spatial frequencies of the phase reversal) of the measured and convolved ITF as described above in this section. In addition, we have investigated whether adding simple correction terms to the circular-aperture model can be beneficial. We have found empirically that the addition of a cubic term significantly improves the approximation to the true ITF:

$$ITF_{NOM} = \frac{J_1(2\pi a u)}{\pi a u}\left(1 + C \cdot u^3\right). \tag{14}$$

We call the ITF given by Eq. (14) the 'NOM approximation' ITF.

The optimal value of the parameter C is $C \approx 3.7 \cdot 10^{-6}\,\mathrm{mm}^{-3}$, found by minimizing the rms of the difference between the measured and convolved inherent slope traces. Note that the fitting parameter C affects only the amplitude rather than the phase properties of the ITF. This allows us to independently optimize the both fitting parameters a and C in Eq. (14).

The results of the optimization are presented in Figs. 1 and 5. In both the spatial (Fig. 1) and spatial-frequency (Fig. 5) domains, the measured and the convolved traces are almost perfectly matched. This is a validation of the obtained empirical approximation of the ITF of an AC ELCOMAT-3000 based profiler equipped with a circular aperture of 2.5-mm diameter.

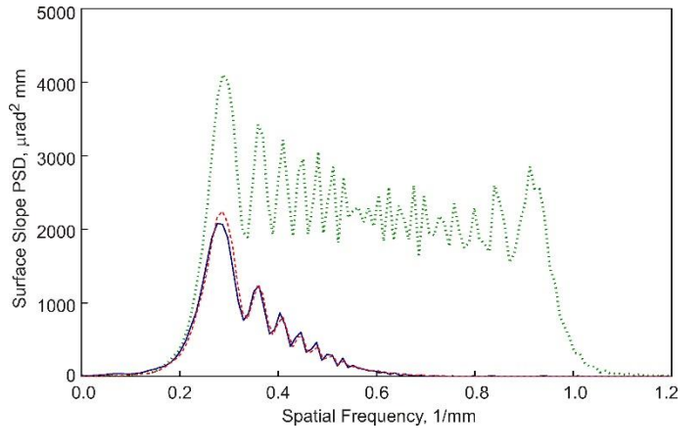

Fig. 5. The PSD of the slope distributions of the chirped sample as measured with the OSMS (the blue solid line) and (the red dashed line) resulting from the convolution of the inherent chirped slope distribution with the NOM approximation ITF. For a reference, the PSD of the inherent chirped slope trace is shown with the green dotted line.

C. Optimization of the regularization parameter

With the OSMS approximation ITF given by Eq. (14) with the optimized parameters $2a = 1.456\,\mathrm{mm}$ and $C \approx 3.7 \cdot 10^{-6}\,\mathrm{mm}^{-3}$, we can optimize the regularization parameter of the Wiener optimal filter, which is used by the SlopeReconstruction1D™ software for 1D data reconstruction in the 'Deconvolve measured' operation mode.

Physically, the regularization parameter accounts for *a priori* unknown PSDs of the signal and instrument noise (see, for example, Ref.[49] and discussion in Sec. II B). The smaller the noise, the smaller the regularization parameter that can be employed, allowing the signal to be recovered at higher spatial frequencies. If the value of the regularization parameter is too small, the effect of the noise appears as strong irregularities in the reconstructed data, clearly seen in both the spatial and spatial frequency domains. Here, as a measure of the regularization success, we use the rms variation of the difference between the inherent and reconstructed slope profiles of the chirped sample. The minimum of the rms variation corresponds to the best possible matching of the PSD spectra of the profiles.

Figure 6 presents, in the spatial frequency domain, the results of partial reconstruction of the chirped-sample surface slope variation possible from the data measured with the OSMS.

In Fig. 6, the PSD distribution of the measured and the inherent slope profilers are shown with the dashed blue and dotted green lines, respectively; the PSDs of the reconstructed traces are depicted with the solid red lines. For the reconstruction, we used the NOM approximation ITF, defined by Eq. (14) with $a = 0.728\,\text{mm}$ and $C \approx 3.7 \cdot 10^{-6}\,\text{mm}^{-3}$, and different values of the regularization parameters, –0.1, –0.3, and –0.5.

Within the selected range of the regularization parameters of [–0.1, –0.5], the PSDs of the reconstructed data in Fig. 6 are almost independent of the parameter for spatial frequencies up to approximately 0.5 mm^{-1}. However, at spatial frequencies between 0.5 mm^{-1} and 0.6 mm^{-1} (the range denoted in Fig. 6 with the arrows), the matching of the PSDs is slightly better at the regularization parameter of –0.5. The demonstrated weak dependence of the reconstruction result on the value of the regularization parameter over a factor of 5 variation shows that reconstruction

parameters determined from calibration measurements can be usefully applied to metrology data obtained for high-quality x-ray mirrors.

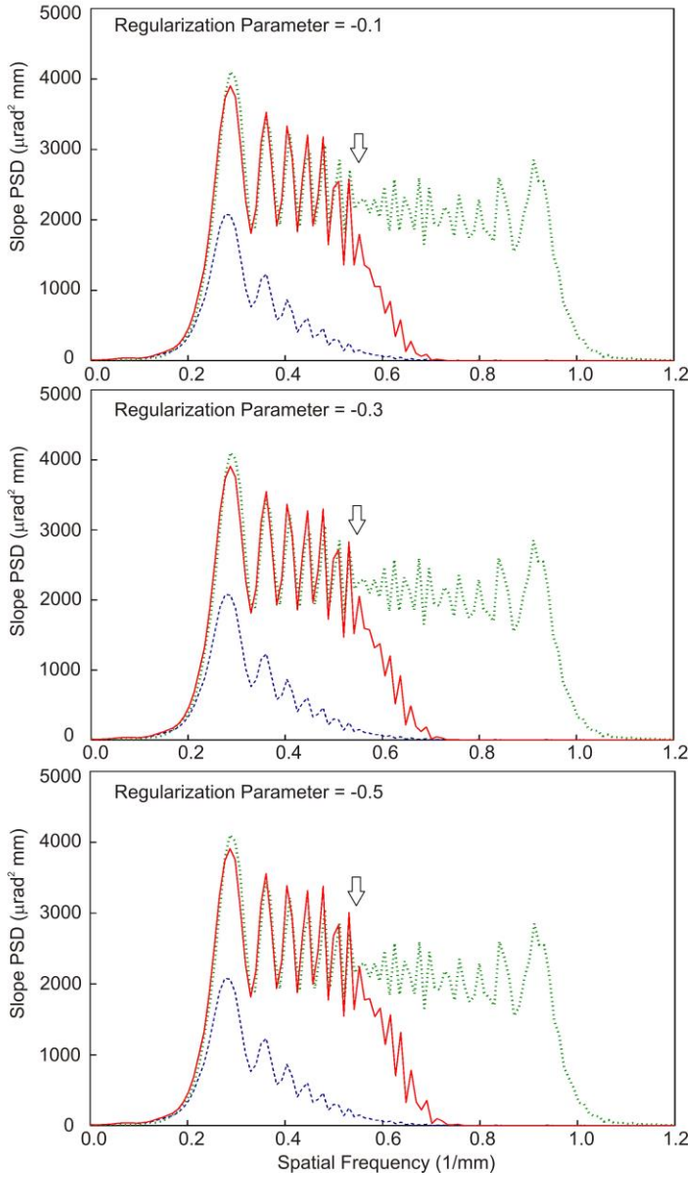

Fig. 6. (The blue dashed lines) The PSD of the surface slope variation of the chirped test sample as measured with the OSMS with the increment of 0.1 mm; (the red solid lines) the PSDs of the slope traces reconstructed from the measured trace with the OSMS approximation ITF; the inherent slope profilers are shown with the dotted green lines. Different values of the regularization parameter, shown in each plot, were used in the 'Deconvolve measured' operation mode of the SlopeReconstruction1D™ software. The arrows depict the spatial frequency range where the PDS spectra are noticeably different.

In the spatial domain, the quality of matching the inherent and the reconstructed slope traces is illustrated in Fig. 7 for the case of the regularization parameter of −0.5, corresponding to the PSD data in Fig. 6(c). The value of the regularization parameter of −0.5 is used in Sec. IV for reconstruction of the OSMS data obtained with state-of-the-art elliptical x-ray mirrors.

The example data in Figs. 6 and 7, obtained in the course of the OSMS calibration, can also be thought of as an illustration of the efficacy of the reconstruction of the slope data measured with the XROL OSMS with 2.5-mm diameter aperture.

In summary of this section, the developed reconstruction technique and software allows reliable recovery of the surface slope variations of the chirped test sample profile with spatial frequencies up to approximately 0.6 mm^{-1} corresponding to spatial periods of about 1.6 mm and longer. Without the reconstruction, the error in the 0.6-mm^{-1} amplitude of the PSD of the original slope data, measured with the OSMS equipped with 2.5-mm aperture (the dashed blue traces in Fig. 6), reaches a factor of approximately 20. Correspondingly, the error in the amplitude of the surface height variation with period of 1.6 mm is a factor of more than 4 (see Fig.7), and the rms variation is increased from 25 μrad to almost 46 μrad.

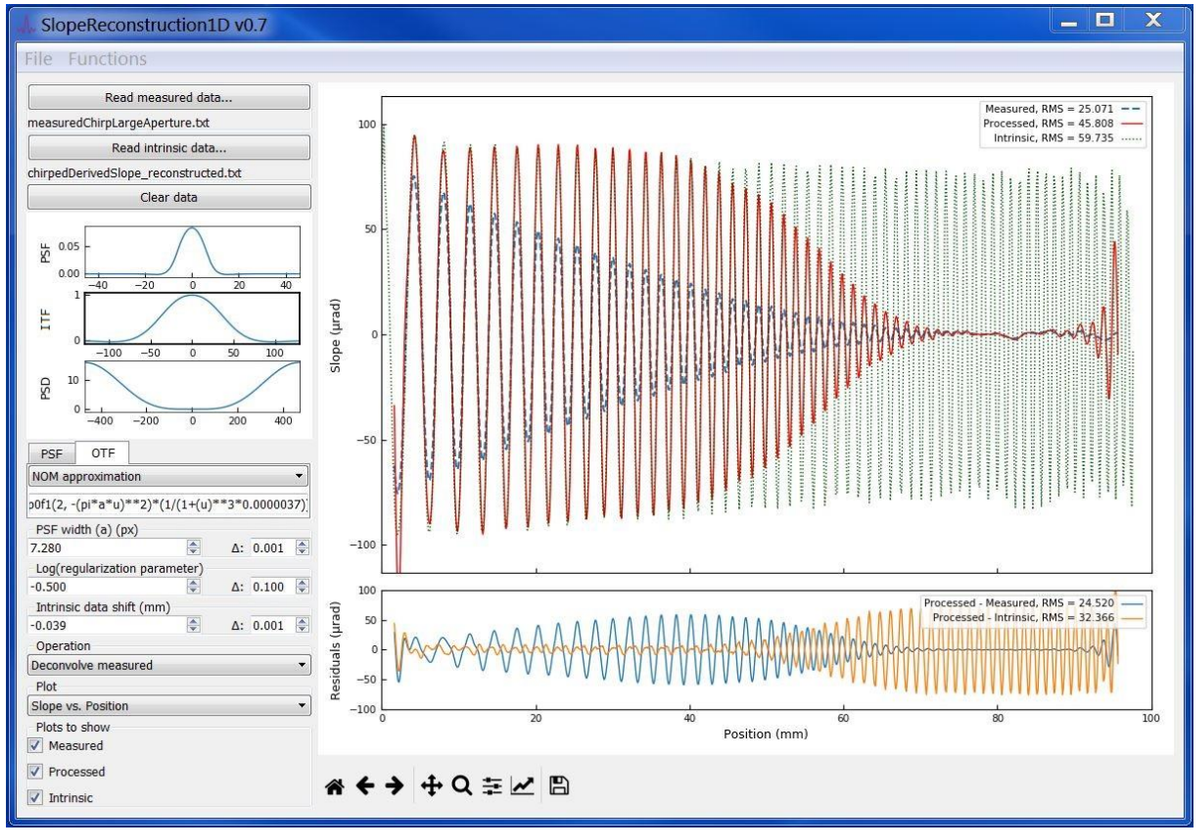

Fig. 7. Application window of the reconstruction software SlopeReconstruction1D™ with the example of reconstruction of the chirped test sample data measured with the OSMS: (the blue dashed line) surface slope distribution measured with the chirped test sample; (the red solid line) the reconstructed slope trace, and (the green dotted line) the inherent chirped slope profile. For the reconstruction, the NOM approximation ITF and the regularization parameter of –0.5 were used.

IV. RECONSTRUCTION TO 1D SLOPE METROLOGY DATA OBTAINED WITH STATE-OF-THE-ART X-RAY ELLIPTICAL MIRRORS

In this section, we apply the reconstruction procedure, optimized in Sec. III, to account for the spurious effect of the OSMS ITF to tangential slope data, obtained with two elliptical-cylinder mirrors, constituting a Kirkpatrick-Baez (KB) focusing pair.[53] The mirrors were fabricated for the ALS micro-diffraction beamline BL 12.3.2[54] by using a deterministic polishing process.

For the measurements with mirrors, the AC ELCOMAT-3000 in the OSMS sample arm was equipped with a circular aperture of 2.5-mm diameter. The high confidence of the OSMS measurements is ensured by the in-situ calibration of the AC; the application of a number of

original experimental techniques for suppression of random, drift, and systematic errors of the measurements; as well as by the usage of distinctive analytical methods and software for data analysis and processing (see Refs.[10,22,23,40,55] and references therein). The absolute accuracy of the tangential slope measurements with the BL 12.3.2 mirrors is estimated to be on the level of 30 nrad rms.

A. Horizontally focusing mirror

The horizontally focusing mirror (HFM) is the first in the KB pair. Because of the larger focal distance, it has larger radius of curvature, varying from ~110 m to ~165 m, and smaller total surface slope variation that is ~0.66 mrad, than that of the vertically focusing mirror (VFM). Accordingly, the specification for the surface slope error of the HFM, <100 nrad rms, is twice as stringent.

Figure 8 shows, with the blue solid lines, the residual slope variation of the HFM and its PSD, as measured with the OSMS and, with the red dashed lines, the result of reconstruction of the measured data.

The OSMS metrology (the blue solid line in Fig. 8a), performed with 0.2-mm increment along the sagittal center of the mirror, has confirmed the super high quality of the optic. The measured residual slope error (after subtraction of the best-fit elliptical shape[40]) is 54 nrad rms; significantly better than the specification. But the reconstructed slope data in Fig. 8a suggests that the residual error of the HFM surface is 61 nrad rms; larger than the originally measured by ~13%.

For the reconstruction, the SlopeReconstruction1D^{TM} software with parameters corresponding to that of the OSMS ITF calibration discussed in Sec. III and depicted in Figs. 6c and 7 was used.

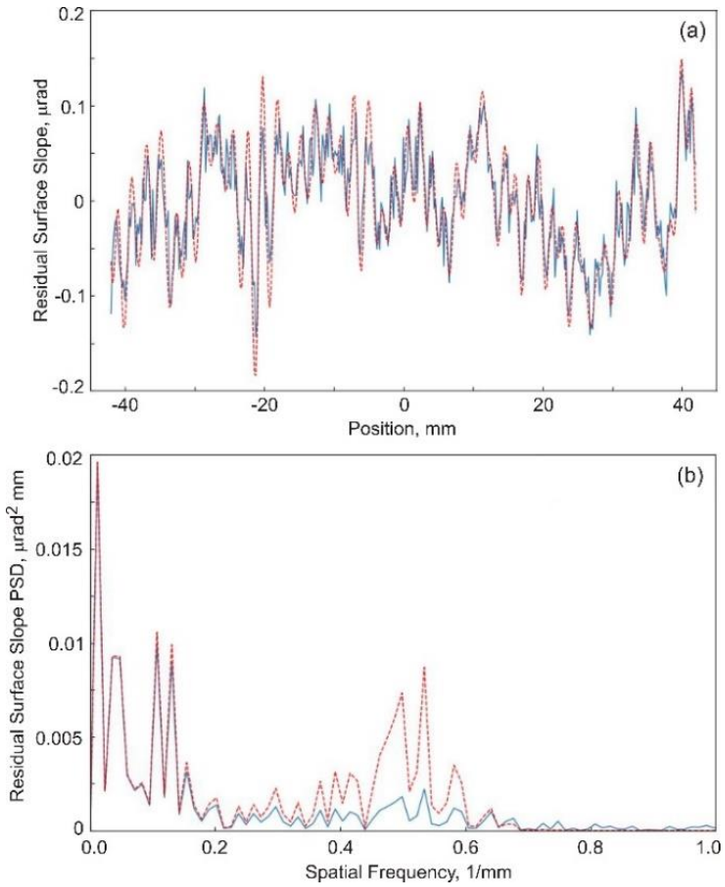

Fig. 8. (a) The HFM residual slope distribution in the tangential direction, as measured with the OSMS with 0.2-mm increment (the blue solid line); and (the red dashed line) the reconstructed slope distribution. (b) The PSD spectra of the measured and the reconstructed slope distributions, shown in plot (a). The OSMS ITF calibration and the parameters of the reconstruction routine correspond to that of discussed in Sec. III and depicted in Figs. 6c and 7.

The most remarkable result of the reconstruction is the increase of the PSD amplitude of the quasi-periodic perturbation at the spatial frequencies around 0.5 mm^{-1} by a factor of about 4.5 – Fig. 8b. Such quasi-periodic surface slope errors are very characteristic of the modern deterministic polishing processes used for fabrication of aspherical x-ray mirrors.[40,41]

B. Vertically focusing mirror

The vertically focusing mirror (VFM) is the second in the KB pair. Because of a twice smaller focal distance, the VFM is very curved with the radius of curvature varying from ~47 m to ~100 m.

Correspondingly, the total surface slope variation over the clear aperture of 85 mm is ~1.3 mrad. The surface slope error of the VFM is specified to be < 200 nrad rms.

The results of the OSMS measurements and the reconstruction of the surface slope distribution of the VFM are depicted in Fig. 9. In the case of the VFM, the measurement arrangement and the reconstruction parameters are the same as for the HFM.

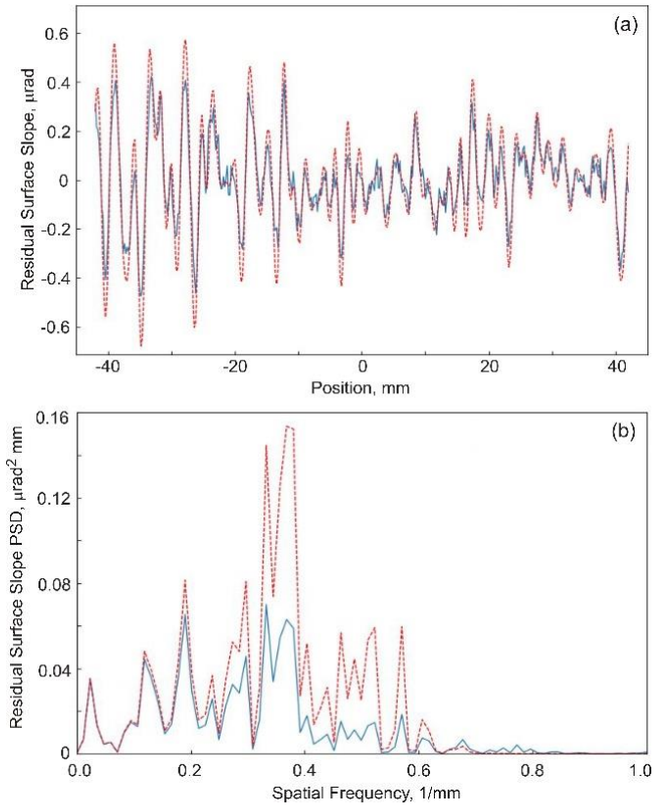

Fig. 9. (a) The VFM residual slope distribution in the tangential direction, as measured with the OSMS (the blue solid line); and (the red dashed line) the reconstructed slope distribution. (b) The PSD spectra of the measured and the reconstructed slope distributions, shown in plot (a). The arrangement of the measurements and the parameters of the reconstruction are the same as in the case of the HFM (Fig. 8).

The reconstructed residual slope trace of the VFM (Fig. 9a) has the rms variation of 213 nrad. This should be compared with the value of 159 nrad rms obtained from the raw (measured) slope data.

Analogous to the HFM, the reconstruction of the VFM data reveals significantly larger PSD amplitudes of the quasi-periodic perturbations: by a factor of ~ 2.5 at the spatial frequencies around 0.35 mm^{-1}, and by a factor of ~ 4 at the frequencies around 0.5 mm^{-1} – Fig. 9b.

Completing the discussion of the reconstruction of the 1D surface slope topography of these two mirrors, we should note that the reconstruction provides more reliable data not only over the spatial frequency range below ~ 0.6 mm^{-1}, determined by the OSMS ITF (compare with Figs. 6 and 7), but also at the spatial frequencies > 0.7 mm^{-1}, where the random error of the measurements is effectively filtered out by the reconstruction.

VI. CONCLUSIONS

In this work, we have discussed experimental, analytical, and numerical methods constituting a multistep procedure developed for super-resolution surface slope metrology of x-ray mirrors. The developed procedure allows partial reconstruction of 1D surface slope topography, inherent to the x-ray mirrors under test, over the spatial frequency range where the raw data are significantly perturbed due to the limited resolution of the slope profiler in use. The developed procedure is based on the measured and analytically modeled ITF of the profiler.

We have empirically derived and experimentally verified analytical expressions for the ITF of the XROL OSMS,[10,22,23] a surface-slope profiler based on an autocollimator ELCOMAT-3000 with 2.5-mm-diameter aperture, such as many profilers at x-ray metrology labs.[27-35]

We have outlined an experimental procedure and a sequence of numerical simulations with the developed software that allows us to optimize the parameters of the effective ITF of the profiler, as well as the parameters of the reconstruction routine. The optimization procedure utilizes the experimental data on the profiler's PSF (ITF), obtained in the precision calibration of the OSMS with the chirped slope test sample.[10]

Applying the reconstruction procedure to the resolution calibration data for the OSMS, we have shown that in the case of autocollimator-based slope profilers with a circular aperture of 2.5-mm diameter, the reconstruction recovers surface slope variations with spatial frequencies significantly higher, by a factor of ~2 or more, than that of the original uncorrected data.

The application of the developed methods and software to the surface slope topography of two state-of-the-art aspherical x-ray mirrors, described in this paper, has confirmed a substantial improvement of the accuracy of the final (after reconstruction) results of slope metrology. In the case of these two mirrors, in addition to an increase of the rms error by a factor of up to ~1.3, the reconstruction has revealed significantly larger PSD amplitudes (up to a factor of 4-4.5 at the spatial frequencies around 0.5 mm^{-1}) of the quasi-periodic perturbations of the surface slope topography than that of the original experimental data. Such quasi-periodic surface slope errors can lead to a noteworthy degradation of performance of beamlines, especially those employing coherent x-rays, where the perturbations can lead to increased speckle-like intensity variation.

We believe that the reconstruction technique described in our paper is vital for advanced surface slope profilometry, providing one of a few opportunities to increase the lateral resolution of the metrology data needed for optical fabrication and optimal usage of the optics, and for sophisticated performance simulation of new beamlines and those under upgrade at x-ray facilities. Indeed, when designing new x-ray beamlines, existing optical surface topography data (namely PSD spectra measured with similar optics fabricated with the same polishing technology as those in the design) are often used to forecast the quality of the prospective optics studied to evaluate performance of the beamline under development. However, significant errors in the assessment of the quality of the measured optics, and therefore in the quality of the forecast optics and in the

beamline design, are possible if the perturbation of the measured PSD spectra by the instrument's transfer function is not properly accounted for.

The effect on beamline performance due to an underestimate in surface slope errors for a particular mirror is specific to the mirror's application and the beamline design. A detailed analysis of this influence is out of the scope of this article.

In conclusion, we are currently working on a Phase II project with the goal of extending the approaches and software developed for 1D metrology data reconstruction to the case of 2D data, available, for example, from Fizeau interferometers and interferometric microscopes.

ACKNOWLEDGMENTS

The authors are grateful to Peter de Groot, Wayne McKinney, Peter Takacs, Anastasia Tyurina, and Yury Tyurin for useful discussions. This work was performed in the scope of the subcontract with Rochester Scientific, LLC, supported by the U.S. Department of Energy STTR program on industrialization of the BPRA based MTF calibration technique under Award Numbers DE-SC0011352 to aBeam Technologies, Inc. Research at the Advanced Light Source and the Molecular Foundry at Lawrence Berkeley National Laboratory are DOE Office of Science User Facilities under contract no. DE-AC02-05CH11231.

The data that support the findings of this study are available from the corresponding author upon reasonable request.

REFERENCES

[1] V. V. Yashchuk, G. Centers, Yu. N. Tyurin, and A. Yu. Tyurina, Proc. SPIE **9962**, 99620G (2016).

[2] Y. V. Yashchuk, and V. V. Yashchuk, Opt. Eng. **51**(4), 046501 (2012).

[3] V. V. Yashchuk, Y. N. Tyurin, and A. Y. Tyurina, Proc. SPIE **8848**, 88480H (2013).

[4] V. V. Yashchuk, Y. N. Tyurin, and A. Y. Tyurina, Opt. Eng. **53**(8), 084102 (2014).

[5] V. V. Yashchuk, Y. N. Tyurin, and A. Y. Tyurina, Opt. Eng. **55**(7), 074106 (2016).

[6] P. Rose, Y. Surrel, and J. M. Becker, Meas. Sci. Technol. **20**, 095110 (2009).

[7] F. Siewert, J. Buchheim, T. Höft, T. Zeschke, A. Schindler, and T. Arnold, Nucl. Instrum. Methods A **710**, 42 (2013).

[8] F. Siewert, J. Buchheim, T. Zeschke, T. Arnold, H. Paetzeld, and V. V. Yashchuk, Abstract to The International Workshop on Metrology for X-ray Optics, Mirror Design, and Fabrication, Satellite Workshop at the 12th International Conference on Synchrotron Radiation Instrumentation, SRI 2018 (Berkeley, USA, July 13-16, 2015).

[9] F. Siewert, T. Zeschke, T. Arnold, H. Paetzold, and V. Yashchuk, Rev. Sci. Instrum. **87**(5), 051907 (2016).

[10] I. Lacey, R. D. Geckeler, A. Just, F. Siewert, T. Arnold, H. Paetzelt, B. V. Smith, V. V. Yashchuk, Rev. Sci. Instrum. **90**(2), 021717 (2019).

[11] V. V. Yashchuk, W. R. McKinney, and P. Z. Takacs, "Test Surfaces Useful For Calibration Of Surface Profilometers," U.S. patent application 20100037674 (18 February 2010); U.S. patent 8,616,044 (31 December 2013).

[12] V. V. Yashchuk, W. R. McKinney, and P. Z. Takacs, Proc. SPIE **6704**, 670408 (2007); Opt. Eng. **47**(7), 073602 (2008).

[13] S. K. Barber, P. Soldate, E. D. Anderson, R. Cambie, W. R. McKinney, P. Z. Takacs, D. L. Voronov, and V. V. Yashchuk, J. Vac. Sci. and Tech. B **27**(6), 3213 (2009).

[14] S. K. Barber, E. D. Anderson, R. Cambie, W. R. McKinney, P. Z. Takacs, J. C. Stover, D. L. Voronov, and V. V. Yashchuk, Nucl. Instr. and Meth. A **616**, 172 (2010).

[15] S. K. Barber, P. Soldate, E. D. Anderson, R. Cambie, S. Marchesini, W. R. McKinney, P. Z. Takacs, D. L. Voronov, and V. V. Yashchuk, Proc. SPIE **7448**, 744802 (2009).

[16] S. K. Barber, E. D. Anderson, R. Cambie, S. Marchesini, W. R. McKinney, P. Z. Takacs, D. L. Voronov, and V. V. Yashchuk, Opt. Eng. **49**(5), 053606 (2010).

[17] V. V. Yashchuk, E. H. Anderson, S. K. Barber, N. Bouet, R. Cambie, R. Conley, W. R. McKinney, P. Z. Takacs, and D. L. Voronov, Opt. Eng. **50**(9), 093604 (2011).

[18] V. V. Yashchuk, R. Conley, E. H. Anderson, S. K. Barber, N. Bouet, W. R. McKinney, P. Z. Takacs, and D. L. Voronov, Nucl. Instr. and Meth. A **649**(1), 150 (2011).

[19] S. Babin, G. Calafiore, C. Peroz, R. Conley, N. Bouet, S. Cabrini, E. Chan, I. Lacey, W. R. McKinney, V. V. Yashchuk, and A. Vladar, J. Vac. Sci. and Technol. B **33**(6), 06FL01 (2015).

[20] V. V. Yashchuk, P. J. Fischer, E. R. Chan, R. Conley, W. R. McKinney, N. A. Artemiev, N. Bouet, S. Cabrini, G. Calafiore, I. Lacey, C. Peroz, and S. Babin, Rev. Sci. Instrum. **86**(12), 123702 (2015).

[21] S. Babin, N. Bouet, S. Cabrini, G. Calafiore, R. Conley, G. Gevorkyan, K. Munechika, A. Vladár, and V. V. Yashchuk, Proc. SPIE **10145**, 1014518 (2017).

[22] I. Lacey, J. Adam, G. Centers, G. S. Gevorkyan, S. M. Nikitin, B. V. Smith, and V. V. Yashchuk, Proc. SPIE **10385**, 103850G (2017).

[23] I. Lacey, K. Anderson, G. P. Centers, R. D. Geckeler G. S. Gevorkyan, A. Just, T. Nicolot, B. V. Smith, and V. V. Yashchuk, Proc. SPIE **10760**, 1076002 (2018).

[24] V. V. Yashchuk, N. A. Artemiev, I. Lacey, W. R. McKinney, and H. A. Padmore, Proc. SPIE **9206**, 92060I (2014).

[25] V. V. Yashchuk, N. A. Artemiev, I. Lacey, W. R. McKinney, and H. A. Padmore, Opt. Eng. **54**(10), 104104 (2015).

[26] MÖLLER-WEDEL OPTICAL, GmbH, "ELCOMAT 3000;" https://www.haag-streit.com/moeller-wedel-optical/products/electronic-autocollimators/elcomat-series/elcomat-3000/.

[27] F. Siewert, T. Noll, T. Schlegel, T. Zeschke, and H. Lammert, AIP Conf. Proc. **705**, 847 (2004).

[28] F. Siewert, J. Buchheim, S. Boutet, G. J. Williams, P.A. Montanez, J. Krzywinski, and R. Signorato, Opt. Express **20**(4), 4525 (2012).

[29] S. G. Alcock, K. J. S. Sawhney, S. Scott, U. Pedersen, R. Walton, F. Siewert, T. Zeschke, F. Senf, T. Noll and H. Lammert, Nucl. Instr. Meth. A **616**(2-3), 224 (2010).

[30] V. V. Yashchuk, S. Barber, E. E. Domning, J. L. Kirschman, G. Y. Morrison, B. V. Smith, F. Siewert, T. Zeschke, R. Geckeler, and A. Just, Nucl. Instr. and Meth. A **616**(2-3), 212 (2010).

[31] I. Lacey, N. A. Artemiev, E. E. Domning, W. R. McKinney, G. Y. Morrison, S. A. Morton, B. V. Smith, and V. V. Yashchuk, Proc. SPIE **9206**, 920603 (2014).

[32] L. Assoufid, N. Brown, D. Crews, J. Sullivan, M. Erdmann, J. Qian, P. Jemian, V. V. Yashchuk, P. Z. Takacs, N. A. Artemiev, D. J. Merthe, W. R. McKinney, F. Siewert, and T. Zeschke, Nucl. Instrum. Meth. A **710**, 31 (2013).

[33] J. Nicolas and J. C. Martınez, Nucl. Instr. and Meth. A **710**, 24 (2013).

[34] S. Qian, R. D. Geckeler, A. Just, M. Idir, and X. Wu, Nucl. Instr. and Meth. A **785**, 206 (2015).

[35] S. Qian and M. Idir, Proc. SPIE **9687**, 96870D (2016).

[36] R. D. Geckeler and A. Just, Proc. SPIE **6704**, 670407 (2007).

[37] F. Siewert, J. Buchheim, and T. Zeschke, Nucl. Instrum. and Meth. A **616**(2–3), 119 (2010).

[38] H. Müller, G. Böhm, and T. Arnold, Proc. SPIE **11171**, 111710A (2019).

[39] V. V. Yashchuk, I. Lacey, T. Arnold, H. Paetzelt, S. Rochester, F. Siewert, and P.Z. Takacs, Proc. SPIE **11109**, 111090M (2019).

[40] V. V. Yashchuk, I. Lacey, G. S. Gevorkyan, W. R. McKinney, B. V. Smith, T. Warwick, Rev. Sci. Instrum. **90**(2), 021711 (2019).

[41] F. Siewert, J. Buchheim, T. Zeschke, M. Stormer, G. Falkenberg, and R. Sankari, J. Synchrotron Rad. **21**, 968 (2014).

[42] N. Wiener, [Extrapolation, Interpolation, and Smoothing of Stationary Time Series], Martino Publishing, Mansfield Centre, CT (2013).

[43] A. M. Grigoryan, E. R. Dougherty, and S. S. Agaian, Signal Processing **121**(C), 111 (2016).

[44] G. D. Boreman, [Modulation Transfer Function in Optical and Electro-optical Systems], SPIE Press, Bellingham, Washington (2001).

[45] S. M. Kay, [Modern Spectral Estimation: Theory and Application], Prentice Hall, Englewood Cliffs (1988).

[46] G. M. Jenkins and D. G. Watts, [Spectral Analysis and its Applications], Fifth Printing: Emerson-Adams Press, Boca Raton (2007).

[47] B. Davies, [Integral Transforms and their Applications], 3rd ed., Springer, (2002); p. 28: "Heaviside step function."

[48] R. L. Easton, [Fourier methods in imaging], 1st ed., Wiley (2010); Ch. 19: "Applications of linear filters."

[49] J. S. Lim, [Two-dimensional signal and image processing], P.T.R. Prentice-Hall, Englewood Cliffs (2010); Ch. 9: "Image restoration."

[50] A. Savitzky and M. J. E. Golay, Anal. Chem. **36**, 1627 (1964).

[51] J. Campos, L. P. Yaroslavsky, A. Moreno, and M. J. Yzuel, Opt. Lett. **27**(22), 1986 (2002).

[52] R. Geckeler (PTB, Germany), private communication.

[53] P. Kirkpatrick and A. V. Baez, JOSA **38**(9), 766 (1948).

[54] The ALS BL12.3.2; https://sites.google.com/a/lbl.gov/bl12-3-2.

[55] V. V. Yashchuk, G. Centers, G. S. Gevorkyan, I. Lacey, and B. V. Smith, Proc. SPIE **10612**, 106120O (2018).

SlopeReconstruction1D v0.7

File Functions

Read measured data...

measuredChirpLargeAperture.txt

Read intrinsic data...

chirpedDerivedSlope_reconstructed.txt

Clear data

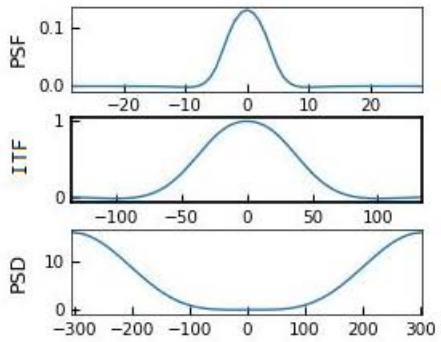

PSF OTF

NOM approximation

0f1(2, -(pi*a*u)**2)*(1/(1+(u)**3*0.0000037))

PSF width (a) (px)

4.525 Δ: 0.001

Log(regularization parameter)

-0.500 Δ: 0.100

Intrinsic data shift (mm)

-0.039 Δ: 0.001

Operation

Convolve intrinsic

Plot

Slope vs. Position

Plots to show

- [x] Measured
- [x] Processed
- [x] Intrinsic

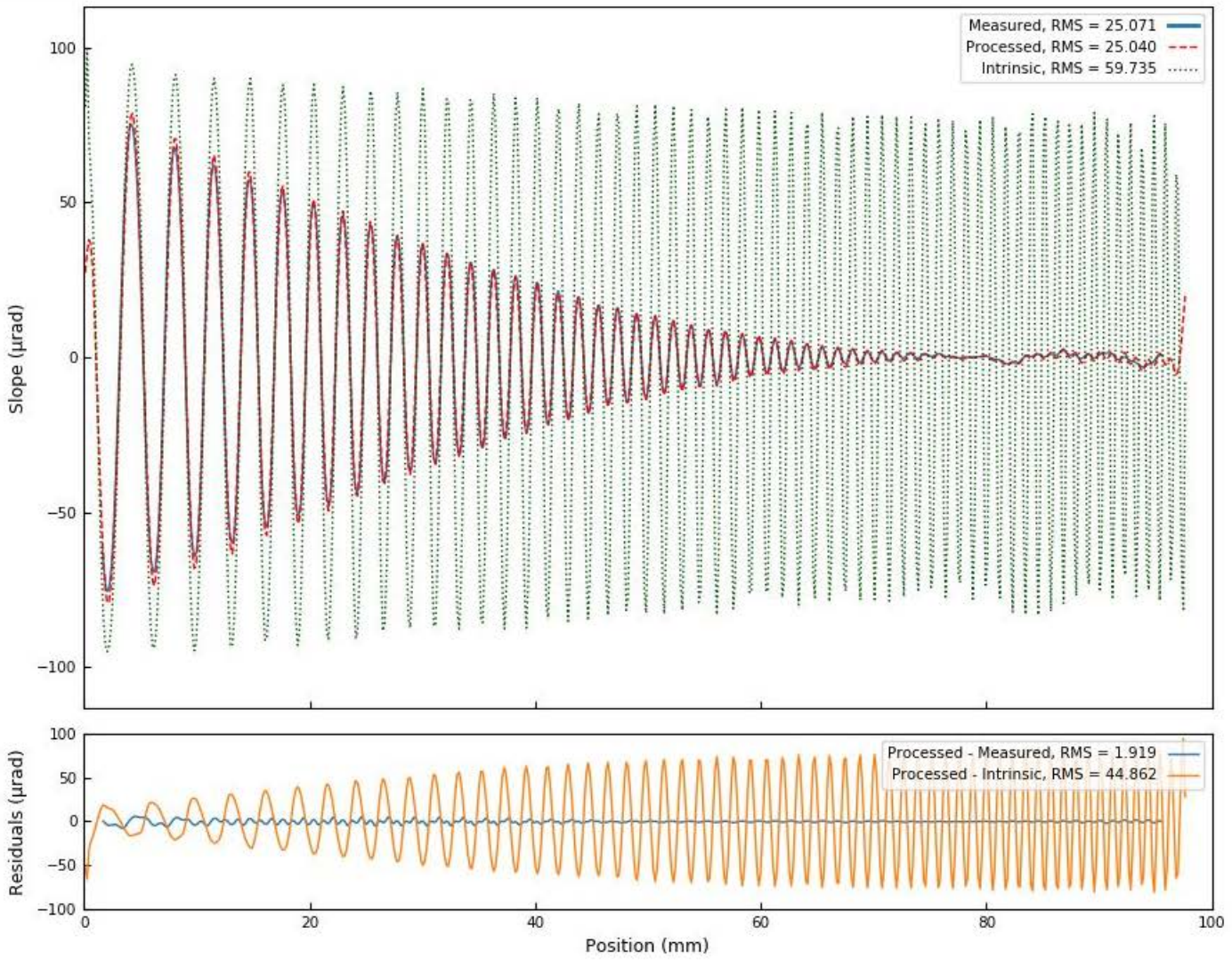

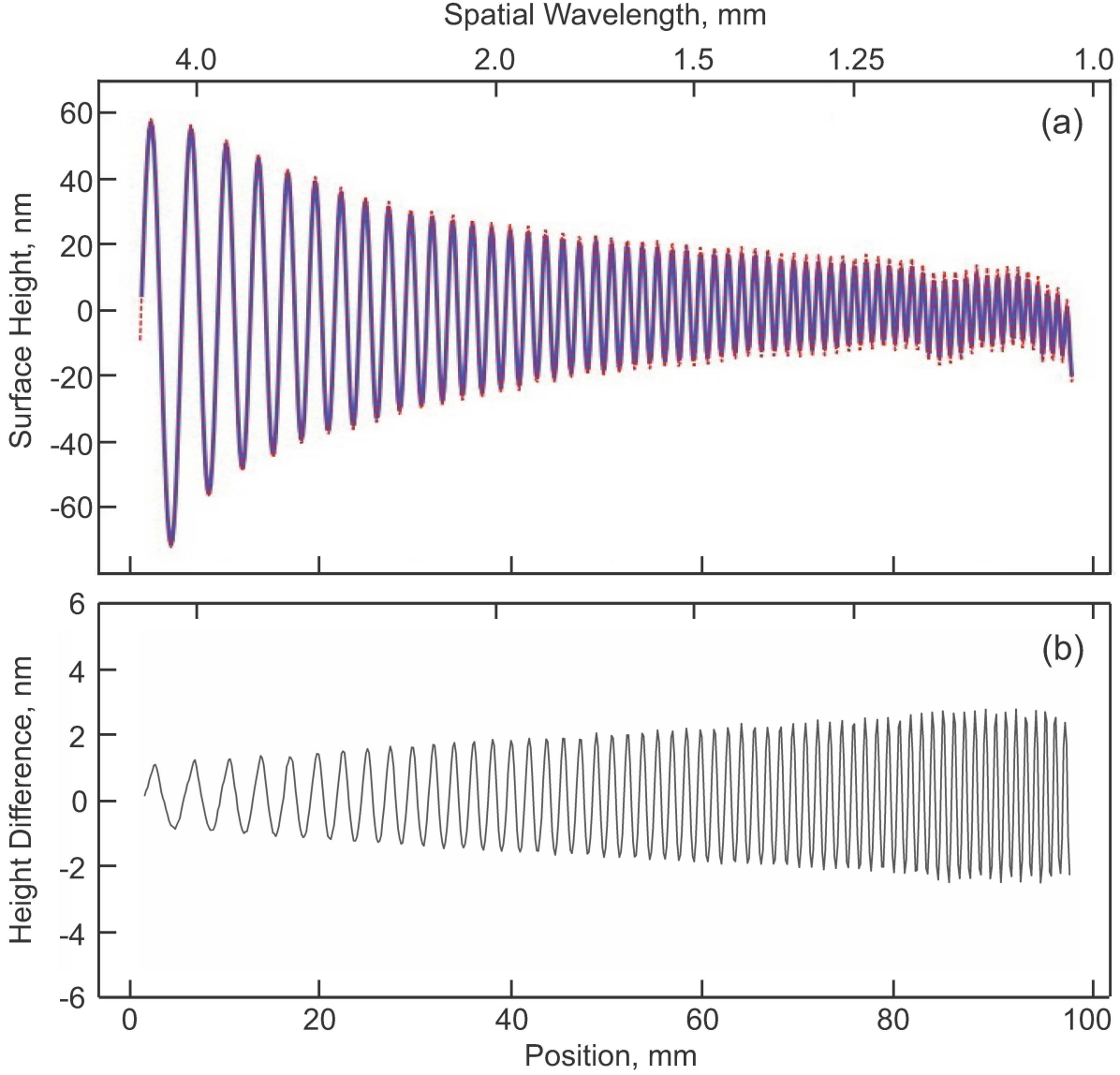
Spatial Wavelength, mm
4.0
2.0
1.5
1.25
1.0
(a)
Surface Height, nm
60
40
20
0
-20
-40
-60
(b)
Height Difference, nm
6
4
2
0
-2
-4
-6
0
20
40
60
80
100
Position, mm

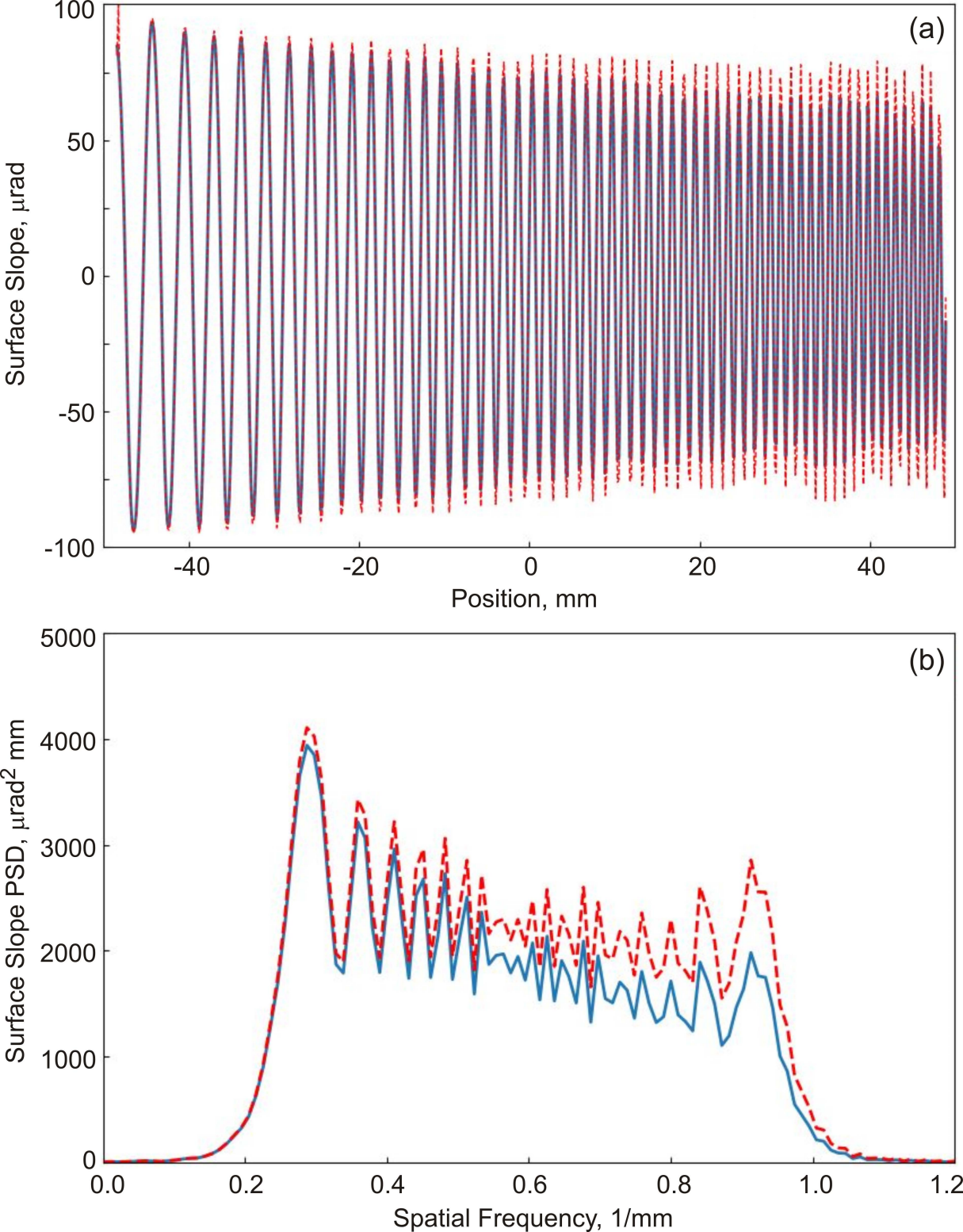
(a)
Surface Slope, µrad
100
50
0
-50
-100
-40
-20
0
20
40
Position, mm
(b)
Surface Slope PSD, µrad^2 mm
5000
4000
3000
2000
1000
0
0.0
0.2
0.4
0.6
0.8
1.0
1.2
Spatial Frequency, 1/mm

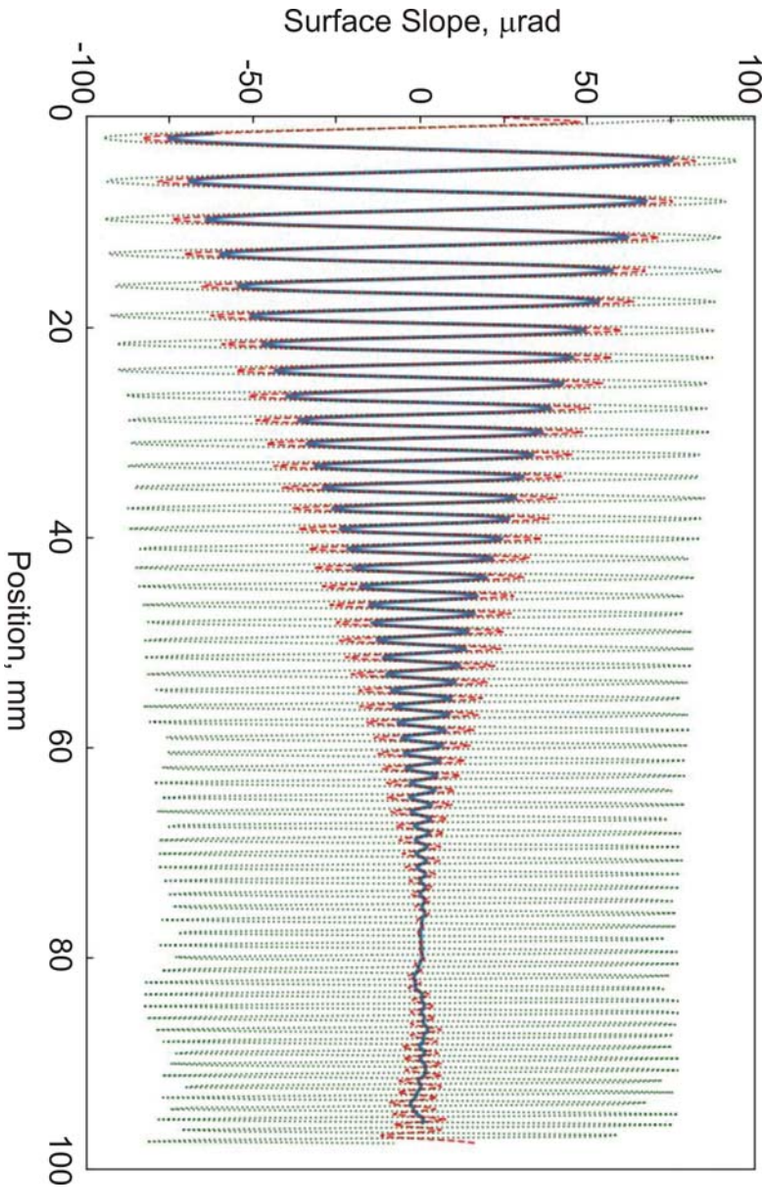

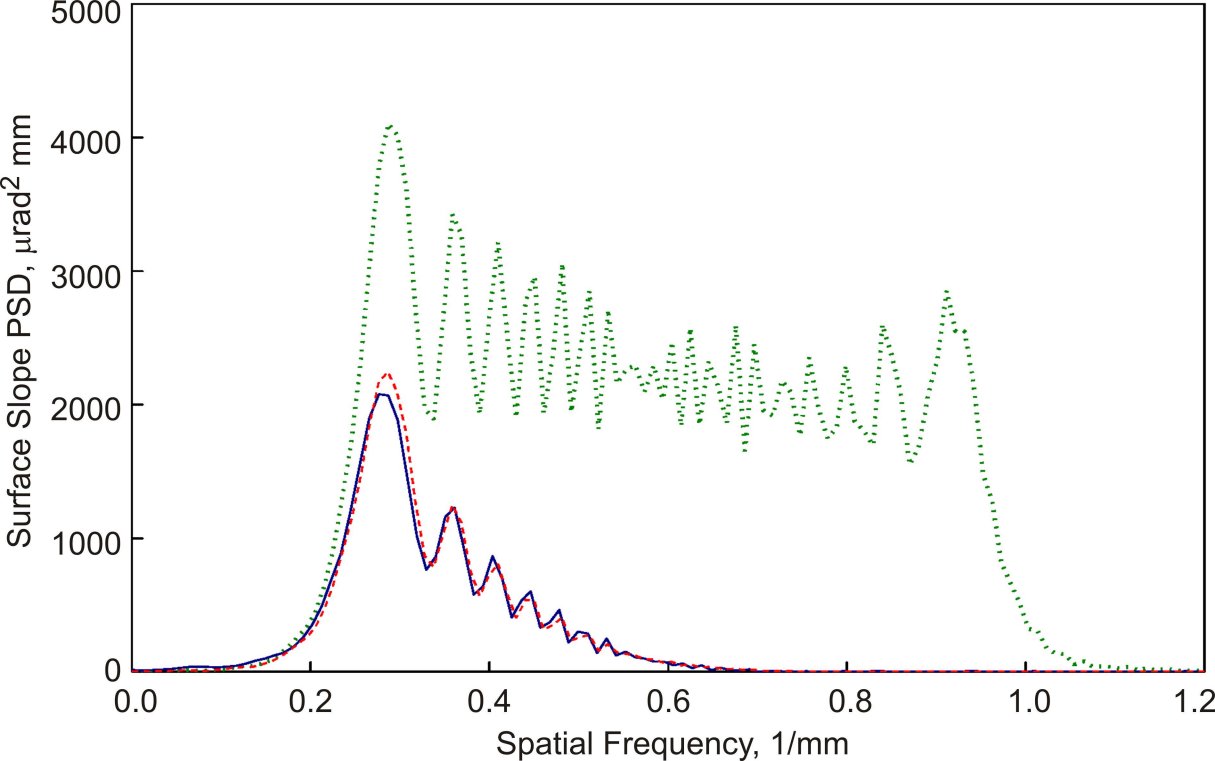
5000
4000
3000
2000
1000
0
Surface Slope PSD, μrad² mm
0.0
0.2
0.4
0.6
0.8
1.0
1.2
Spatial Frequency, 1/mm

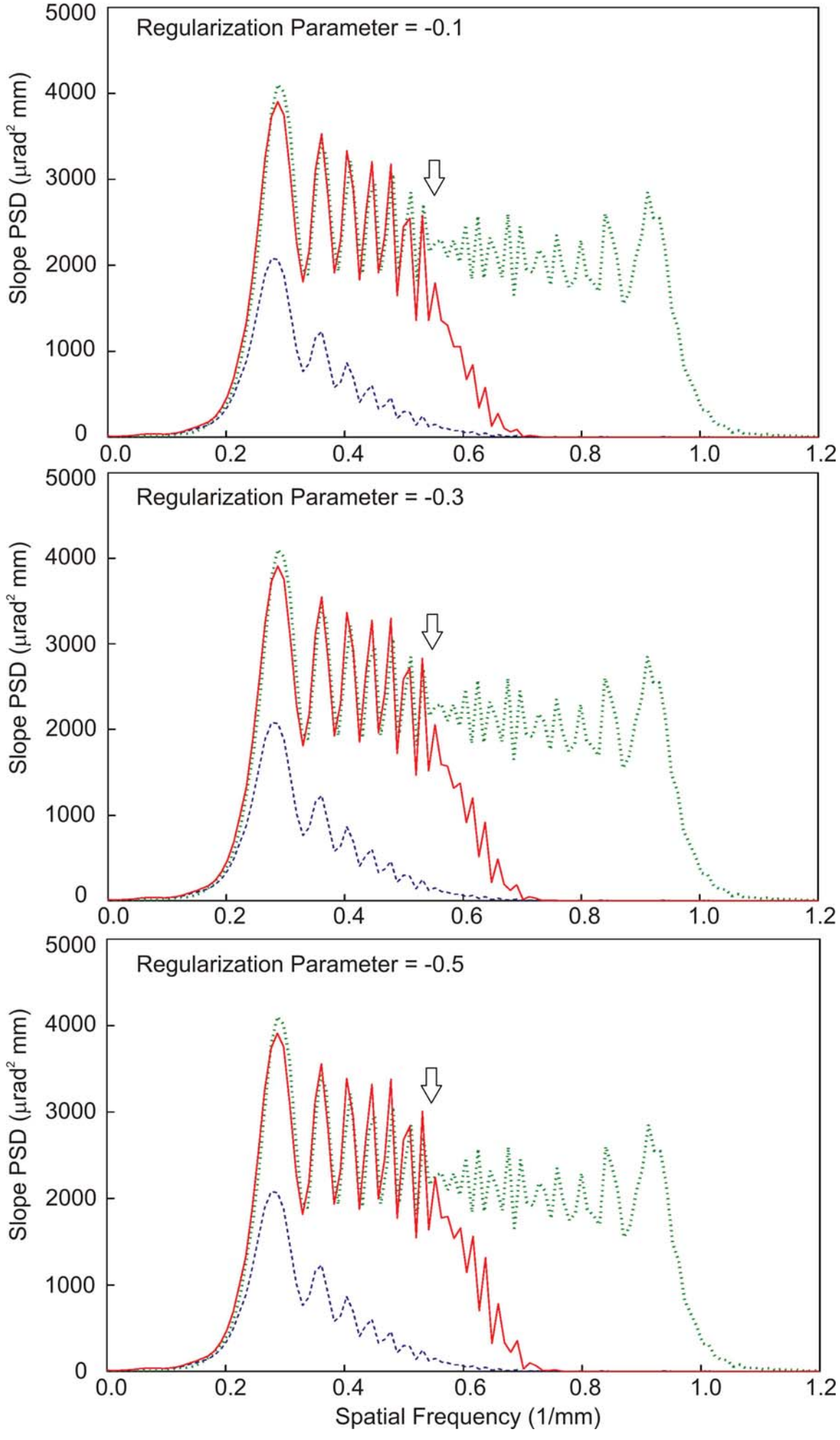

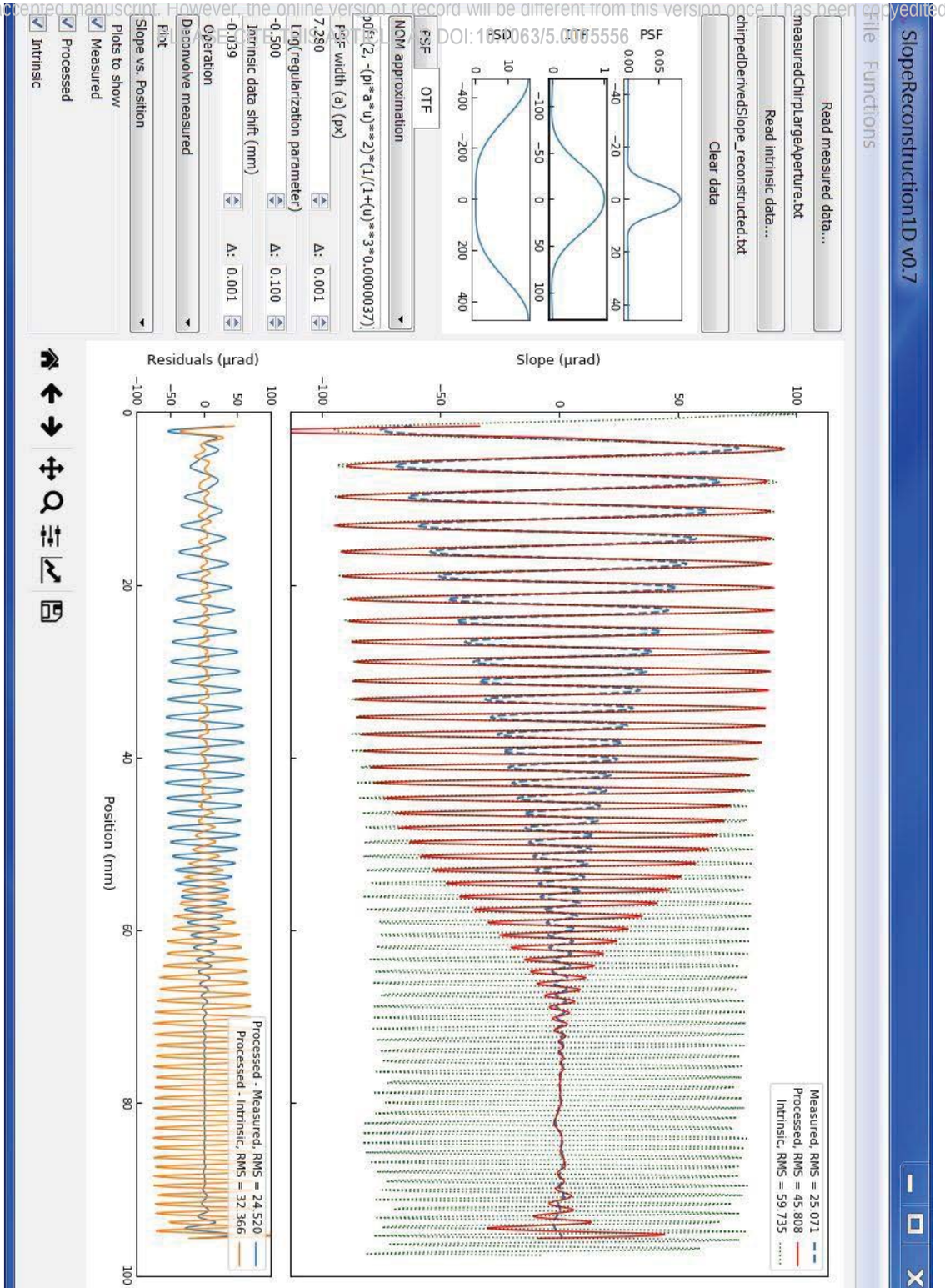

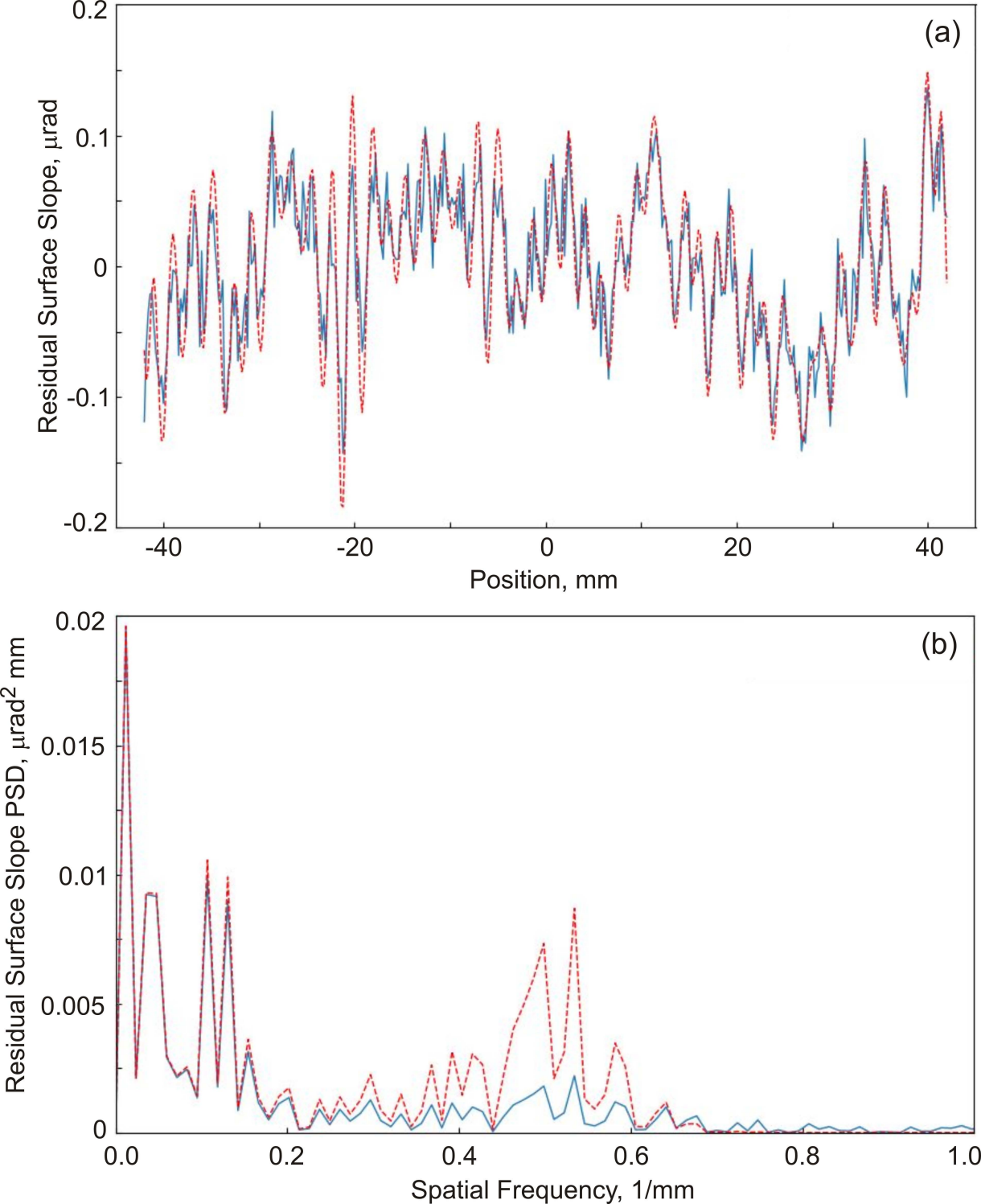
(a)
Residual Surface Slope, µrad
0.2
0.1
0
-0.1
-0.2
-40
-20
0
20
40
Position, mm
(b)
Residual Surface Slope PSD, µrad² mm
0.02
0.015
0.01
0.005
0
0.0
0.2
0.4
0.6
0.8
1.0
Spatial Frequency, 1/mm

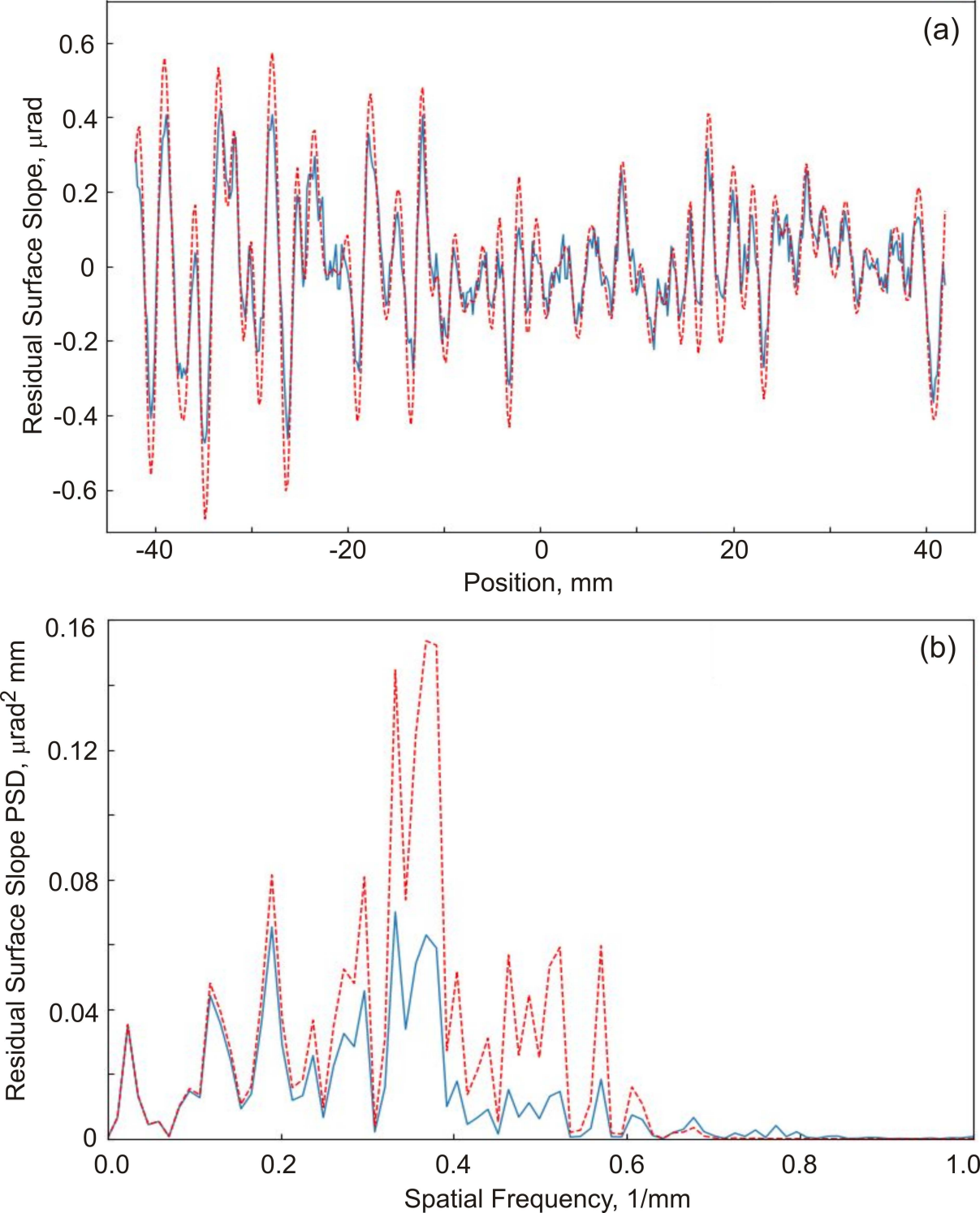
(a)
Residual Surface Slope, μrad
0.6
0.4
0.2
0
-0.2
-0.4
-0.6
-40
-20
0
20
40
Position, mm
(b)
Residual Surface Slope PSD, μrad² mm
0.16
0.12
0.08
0.04
0
0.0
0.2
0.4
0.6
0.8
1.0
Spatial Frequency, 1/mm